LHCb 2004-116 MUON
Created: 18/12/2004

Draft of the Second Addendum to the Muon System Technical Design Report

LHCb Muon Detector Group

Abstract

This note contains draft of the Addendum to the Muon System Technical Design Report describing the detector, based on the triple-GEM technology, which is going to equip region 1 of station 1 of the muon system

1 Introduction

This second addendum to the Muon System Technical Design Report TDR [1][2] is a detailed description of the Triple-GEM detector with pad readout conceived for the inner part (region R1) of the first muon station (M1) of the LHCb experiment.
The LHCb muon system consists of five stations, one of which (M1) is located in front of the electromagnetic calorimeter, while the other four (M2 to M5) are located after the hadronic calorimeter [1].
The muon system provides both the L0 high transverse momentum trigger and the offline muon identification.
The trigger consists of the AND of the five stations, with bunch crossing identification. Each station is segmented in logical pads of four different sizes, increasing with increasing radial distance from the beam axis ; the four different regions, named R1 to R4, are crossed by approximately the same number of triggered muons.
The whole of the muon system is equipped with multi-wire proportional chambers, while for the inner region (R1) of station M1 the LHCb collaboration selected a different technology: the triple-GEM detector.

2 Requirements for the M1-R1 Detector and Technology Choice.

The requirements for station M1-R1 are: a rate capability up to 500 kHz/cm^2 of charged particles (the average rate is 184 kHz/cm^2), more than 96% of efficiency on muons in a 20 ns time window (for bunch crossing identification), a pad multiplicity (which we call cluster size, i.e. the average number of pads above threshold for a minimum ionizing particle crossing the detector at right angle) of less than 1.2 for a pad size of 10 mm$\times$25 mm, a signal width of less than 50 ns to limit the trigger dead time and radiation hardness for 10 years of operation in LHCb.
All these requirements cannot be satisfied by the wire chambers: in particular the efficiency vs. cluster size requirement cannot be met with such small logical pads and the radiation hardness cannot be guaranteed.
During the last three years extensive R&D was performed on GEM detectors by our group (for example, see [3]-[4] and references therein) in order to find a detector configuration and a gas mixture which satisfies the LHCb requirements (see also [5]). The final choice is a triple-GEM detector , with the gas mixture Ar/CO_2/CF_4 (45/15/40).
The layout of the document is as follows: in section 3 the triple-GEM detector is presented together with its optimization for the triggering application. In section 4 prototype construction and tests are discussed and in section 5 the ageing tests are presented.

3 The triple-GEM detector

3.1 Introduction

A GEM (Gas Electron Multiplier) is made by a thin (50 μm) kapton foil, copper clad on each side, with a high surface density of holes. Each hole has a bi-conical structure with external (internal) diameter of 70 μm (50 μm) and a pitch of 140 μm. The bi-conical shape of the hole minimizes the effect of charging-up of the kapton inside the holes and is a consequence of the double mask process used in standard photolitographic technologies.
The GEM foils are manufactured by the CERN-EST-DEM workshop following our global geometrical design.
A typical voltage difference of 350 to 500 V is applied between the two copper sides, giving fields as high as 100 kV/cm into the holes, resulting in an electron multiplication up to a few thousands.

Multiple structures realized by assembling two or more GEMs at close distance allow high gains to be reached while minimizing the discharge probability [6, 3, 5].
The triple GEM detector, which consists of three gas electron multiplier (GEM) foils sandwiched between two conductive planes, can effectively be used as tracking detector, with good time and position resolution performances.
A cross-section of the detector, together with the labeling of the different detector parameters used in this addendum, is shown in Fig. 1. The voltage differences across the various GEM foils are called U_{gem1}, U_{gem2} and U_{gem3} and their sum U^{tot}_{gem}.

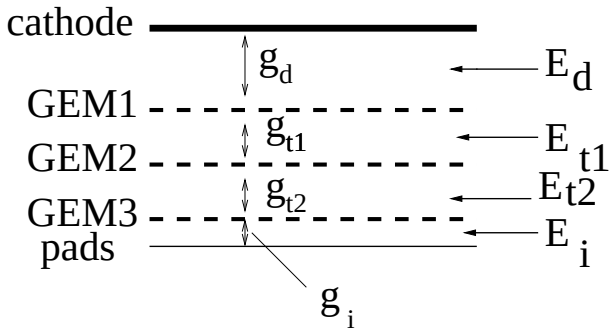

Figure 1 Cross-section of the triple GEM detector. E_d, E_t and E_i are the drift, transfer and induction fields, respectively; g_d, g_{t1},g_{t2} and g_i are the drift, the two transfer and the induction gap, respectively.

3.2 Detector optimization for high rate triggering operation

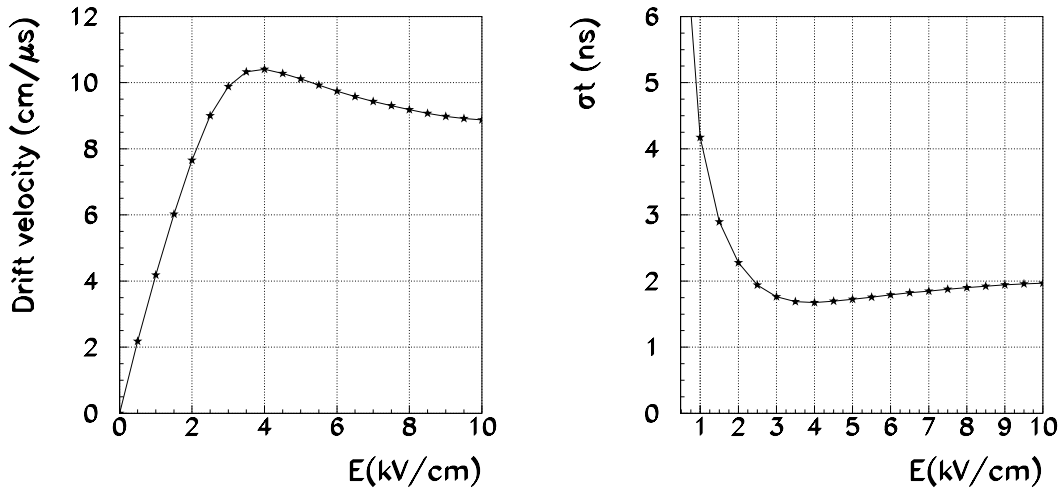

(a) (b)

Figure 2 Calculated electron drift velocity (a) vs. electric field and resolution on the arrival time of primary clusters on the first GEM (b) vs. electric field. A line to guide the eyes through the points is also drawn.

The ionization electrons, produced in the gap between the cathode and the first GEM foil (drift gap) by the charged particles crossing the GEM, are attracted by electric fields through the three GEM foils where they get multiplied. Once they cross the last GEM foil they drift to the anode in the so called induction gap, giving rise to an induced current signal on the pads. With leading edge triggering, the

discriminator crossing on the signal rising edge gives the time of the event.
The number of ionization clusters produced in the drift gap follows a Poisson distribution. The distribution of the cluster closer to one end of the gap is $P(x) = n \cdot exp(-nx)$, which has $\sigma(x) = 1/n$, where n is the average number of ionization clusters per unit length. It follows that, For the cluster closer to the end of gap, which we call the first cluster, $\sigma(t) = 1/(n \cdot v_{drift})$. From a simple calculation it is found that the distribution of the other ionization clusters have a larger $\sigma(t)$, though still proportional to $1/(n \cdot v_{drift})$.
Therefore, the intrinsic time resolution of a triple-GEM detector for incident charged particles scales with $1/(n \cdot v_{drift})$. The best resolution is obtained when the signal corresponding to the first cluster is triggered; this is not always possible due to gain fluctuations but its probability can be maximised by an apropriate choice of detector configuration, i.e GEM fields (gas gain), GEM to GEM fields(transparency of GEM foils to drifting electrons) and, with fast electronics, of detector geometry (pulse height is larger with smaller g_i size).
The occurrence of discharges, i.e. breakdown of gas rigidity, in gas detectors is correlated with the transition from avalanche to streamer occurring when the primary avalanche size exceeds few 10^7 ion-electron pairs, the so called Raether limit. In GEM detectors, due to very small distance between the two sides of the GEM foil, streamer formation can be easily followed by a discharge. This effect can be minimized by both adding a quencher to the gas mixture, whose quantity and type are however limited by detector ageing, and optimizing the detector configuration in order to benefit from the diffusion effect which spreads the charge over more holes.
The above mentioned requirements lead us to select the $Ar/CO_2/CF_4$ (45/15/40) gas mixture, which improves both σ_t and quenching properties with respect to the standard Ar/CO_2 (70/30) one.
Fig. 2(a) shows the drift velocity vs. electric field and Fig. 2(b) the resolution on the arrival time of primary clusters on the first GEM, σ_t, vs. electric field as calculated with Magboltz and Heed programs. The number of primary clusters per incident charged particle is calculated to be 57.3/cm.

3.3 Detector gap and field choice

Detector thickness should be kept to a minimum for both space and performance reasons. However, mechanical considerations indicate that a minimum distance between GEM foils of about 1 mm should be kept.
The drift gap g_d size should be large enough to guarantee full efficiency on charged tracks. The first transfer gap g_{t1} should be kept as small as possible to avoid that primary electrons produced in the same gap give rise to a signal over threshold. A ratio g_d/g_{t1} of 3 was found to be adequate to minimize this effect. The second transfer gap g_{t2} can be larger than the first one to let the diffusion spread the charge over more holes and then lower the discharge probability. The induction gap g should be as small as possible to maximize the signal fraction integrated by the amplifier.
An optimum configuration was found to be, starting from g_d, 3/1/2/1 mm.
The exact values of the fields were found experimentally by optimizing time resolution vs. discharge probability and are E_d=3.5 kV/cm, E_t=3.5 kV/cm and E_i=5 kV/cm.

4 Prototype design and test

4.1 Mechanics

The M1-R1 detector is made of 12 chambers, of active area 20 cm$\times$24 cm, each one consisting of two triple-GEM detectors whose signals are digitally OR-ed. The total active area of the triple-GEM system is 0.6 m^2.
The GEM foils were stretched, with a mechanical tension of about 1 kg/cm with the home-made device shown in Fig. 3. After the GEM stretching, a fiberglass frame is glued on the GEM foil using a Ciba

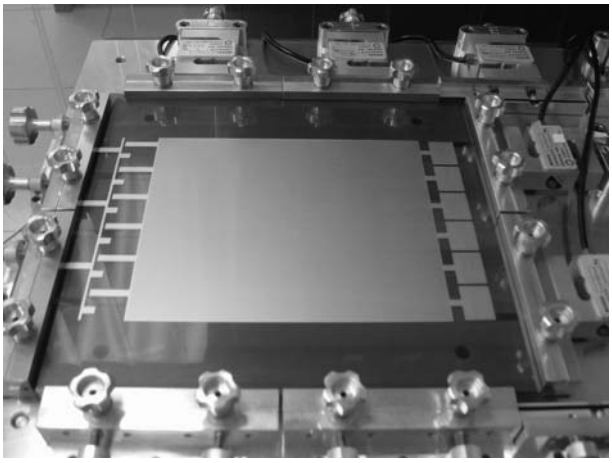

Figure 3 The GEM foil tensioning device. Strain gauges are used to monitor the tension.

2012 epoxy. Both cathode and readout pad electrodes, realized on standard 1.0 mm thick printed circuit board, are respectively coupled with a 1.0 mm fiberglass foil by means of a honeycomb structure, 8 mm thick (in the Module-0 the honeycomb was replaced by a polyurethanic foam). The back-panel with a

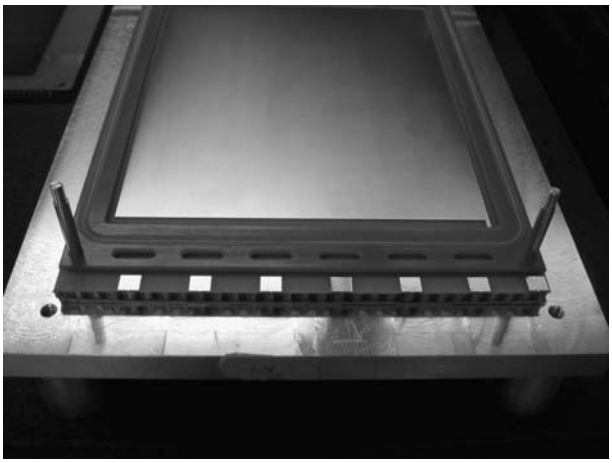

Figure 4 The GEM foil, after gluing on the fiberglass frame, is assembled with the other parts of the detector.

35 μm copper layer deposition on its external side is used as a Faraday cage for the detector. The stiff cathode and pad panels act as support plates for the whole detector. The cathode and pad panels house two gas inlets and two gas outlets, realized with machined delrin inserts. All fiberglass parts that are in contact with the sensitive volume of the detector, are visually inspected in order to find and eliminate any residual spikes or broken fibers, and then cleaned in a ultrasonic bath with de-ionized water and dried in a oven at a temperature of $80\,^{o}$C for one night.

The detector is built piling up and gluing together, on a precision machined reference plane, the single detector parts in the following order: cathode panel; the first GEM foil (GEM1) glued on a 3 mm thick fiberglass frame (see Fig. 4) ; the second GEM foil (GEM2) glued on a 1 mm thick frame; the third GEM foil (GEM3) glued on a 2 mm thick frame and then the last 1 mm thick frame that, followed by the pad panel, defines the induction gap. All the gluing operation are performed using the Ciba 2012 epoxy. Detector dimensions are shown in the cuts of Fig. 5 and Fig. 6. In order to limit the damage in case of discharge, one side of the GEM foil was divided into six sectors, of about 33 mm$\times$240 mm.

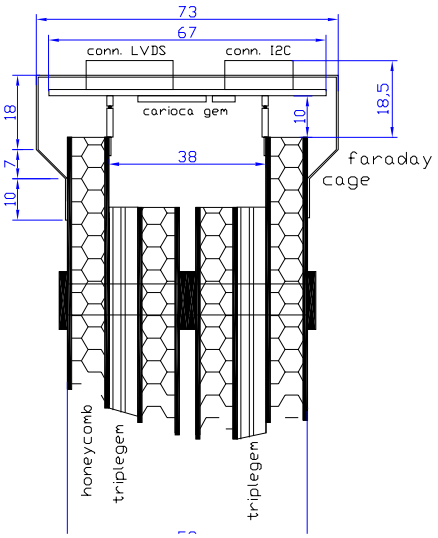

Figure 5 Triple-GEM detector cut with dimensions in mm

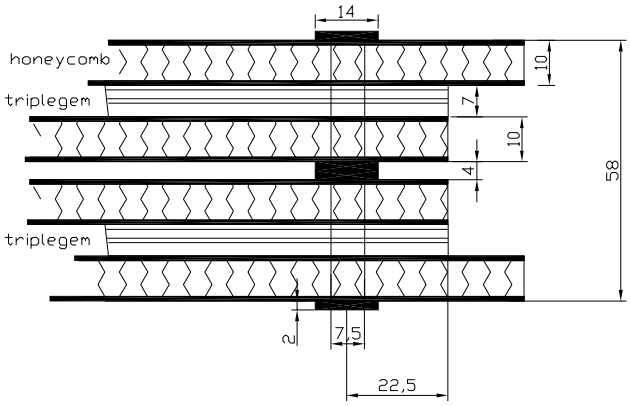

Figure 6 Triple-GEM detector cut with dimensions in mm.

The separation between sectors is 200 μm. For the Module-0, made by two triple-GEM detector whose readout is digitally OR-ed, the high voltage was fed with individual channels to each sector of the top and bottom side of each GEM, and to the cathode through 100 kΩ high voltage resistors. In the final detector a resistive chain will be used to feed the GEM with high voltage.

4.2 Measurement of the effective gain

Effective gain, G_{eff}, vs. U_{gem}^{tot} measurements were performed with a Fe-anode X-ray tube supplied at 20 kV emitting photons at about 6.4 keV[3]. Effective gain values were obtained from the ratio of pad current with high voltage across the GEM foils, to current on the first GEM, with no high voltage across the GEM foils and are shown in figure 7.
Effective gain dependence on U_{gem}^{tot} was obtained from a fit, assuming an exponential behavior. The fitted coefficient is 0.017 V^{-1}.

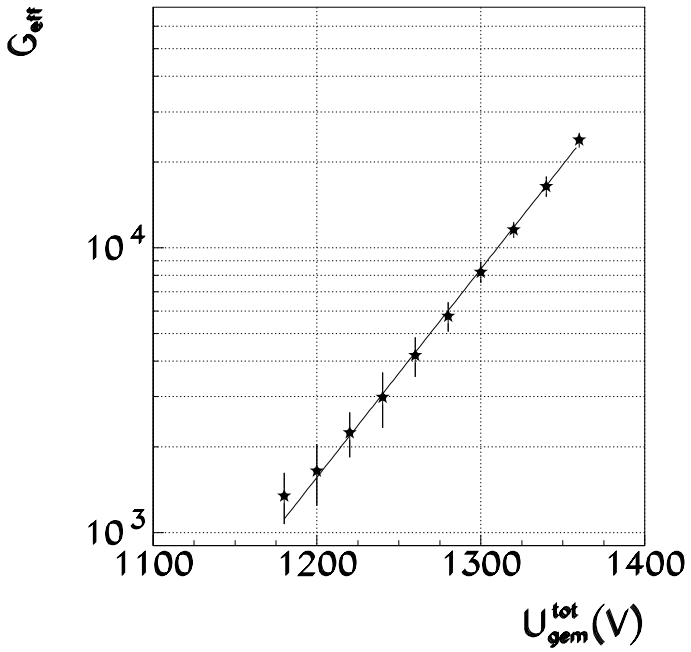

Figure 7 Measured effective gain vs. U^{tot}_{gem}. A fit to an exponential function is superposed to the experimental data.

Reliable detector operation in the experiment is only possible if all requirements in terms of efficiency and detector survival can be satisfied for a certain range of U^{tot}_{gem} or effective gain, in a way that voltage, pressure or temperature variations do not bring the detector outside this range.
Gain dependence on pressure and temperature is expected to be, at the gain values shown in figure 7, ln G=A+B T/P. The parameter B was measured inserting close to the cathode a ^{90}Sr source and was found to be 40 mbar/K.
The efficiency, cluster size and discharge probability measurements will be shown as a function of gain and are meant after T and P correction.

4.3 Electronics

For the triple-GEM Module-0 tests the same amplifiers of the LHCb muon wire chambers were used: the CARIOCA [8] chip (which is the selected one for the wire chambers) and the ASDQ [9] chip. A new version of the CARIOCA chip was designed explicitly for the GEM detector and will be tested soon.
192 channels are needed to readout one detector module. The CARIOCA is an eight channel chip and the front-end boards house two chips per board.

4.4 Measurements of the time performance

The two triple-GEM detectors of Module-0 had two different pad printed circuit boards (PCB): one of the PCB's had a pad to pad distance of 0.4 mm and a ground plane on the other side with a mesh structure, 2 mm pitch and 0.2 mm width, while the other one had a pad to pad distance of 0.6 mm, interleaved by a ground grid of 0.2 mm thickness, without ground plane on the other side. A detailed comparison of the performances in terms of efficiency and cluster size of the two modules, which we omit here for brevity, lead us to select the second type of PCB for the final detector.
The results in terms of the efficiency vs effective gain with the ASDQ readout are shown for the two

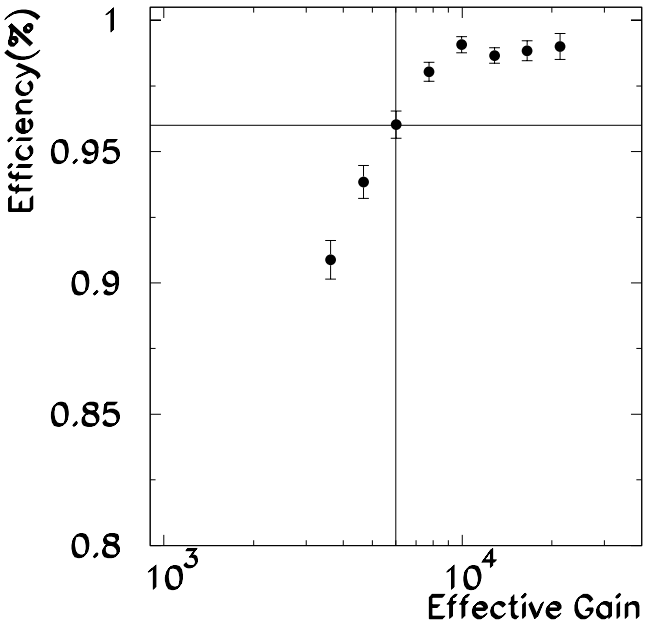

Figure 8 Efficiency of two OR-ed chambers in a 20 ns time window vs. effective gain. The requirement of more than 96% efficiency is shown as an horizontal line; the crossing of this line with the measured efficiency gives the start of the detector plateau.

detectors in OR in Fig. 8 with the threshold set to 2 fC delta pulse equivalent (all the results here are expressed in terms of effective gain, as discussed in [4]). Efficiency measurements, with the same detector, were also performed using the CARIOCA chip. Threshold was set to the minimum allowed in this chip, i.e. 2.5 fC delta pulse equivalent. The effect of the higher threshold is a shift of the efficiency curve of about 30% in terms of the effective gain or 15 V.

Pad cluster size is defined here as the number of pads above threshold per event in a 1×5 pad region around the first triggered pad of the event and in a time window of 20 ns. The probability of having a hit in the 1×5 region above or below the first triggered pad was measured to be less than 2% at any gain.
Fig. 9 shows the pad cluster size vs. the effective gain for the OR of the two chambers.

4.5 Detector plateau

We define, as the start of the plateau (this term is used here with the meaning of an effective gain range of values for which the detector satisfies the LHCb requirements) of the detector, the value of effective gain which corresponds to 96% efficiency. The end of the plateau is defined by the maximum tolerable pad cluster size, i.e. 1.2.
From our results we can say that the plateau in terms of effective gain G_{eff}(end)/G_{eff}(start) is about 3.3, from 6,000 to 20,000. and in terms of high voltage is about 70 V, which is a large plateau for a micro-pattern detector.
The effective gain corresponding to the working point of the detector is at the value of about 6,000.

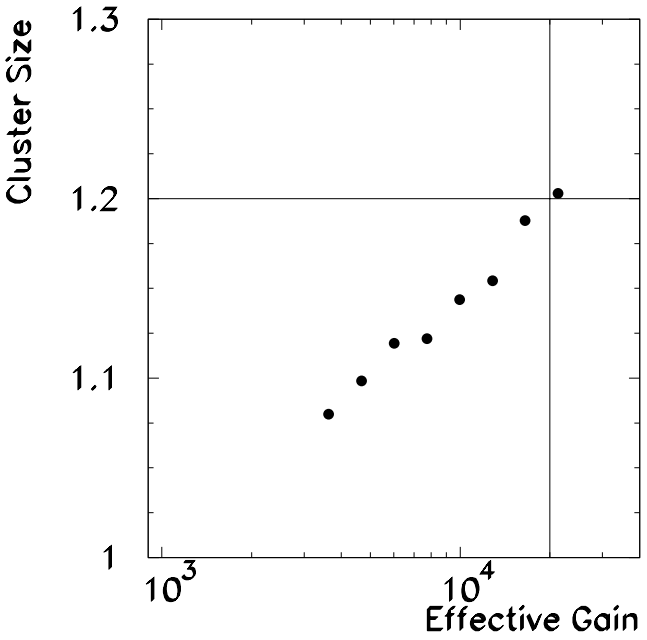

Figure 9 Pad cluster size of two OR-ed chambers vs. effective gain. The requirement of less than 1.2 of cluster size is shown as an horizontal line; the crossing of this line with the measured efficiency gives the end of the detector plateau.

4.6 Sensitivity to high voltage discharges

With micro-pattern detectors the occurrence of discharges has to be accurately studied and monitored since it may lead to detector damage and, eventually, to breakdown.
Therefore, with the selected gas mixture, we measured first the discharge probability per incident particle vs. effective gain with a high-intensity hadron beam, as is described in [4] and shown in Fig. 10.
Then, in the laboratory, with an ^{238}Am α source, we determined the maximum number of discharges the detector can stand before breakdown. The irradiated area was 0.5 cm^2 and the effective gain about 40,000 (more than six times the nominal effective gain). The test was repeated three times and the detectors died after 500, 700 and 800 discharges, respectively. Taking conservatively the first of the three numbers, assuming the average charged particle rate expected in LHCb and 10 years of running, a maximum discharge probability of $5.4 \cdot 10^{-11}$ per incident particle was calculated; from this number and from the results of Fig. 10, a maximum effective gain of about 28,000 for LHCb operation was obtained. This result is conservative since, during the test, the detector was operated at an effective gain much higher than the working point, and detector damage due to a discharge across a GEM hole is very likely to depend on the energy stored in the GEM, which is proportional to the square of the voltage across the GEM.

4.7 Time performance with background radiation

Given the very high particle flux expected in M1-R1, a time performance test was performed in the presence of background radiation.
A large size prototype equipped with ASDQ readout chips was exposed to an intense 1.25 MeV γ ray flux from a ^{60}Co source of the Calliope facility of ENEA-Casaccia. The chamber was placed in a way that radiation flux was not directly coming from the source but after scattering against a wall.

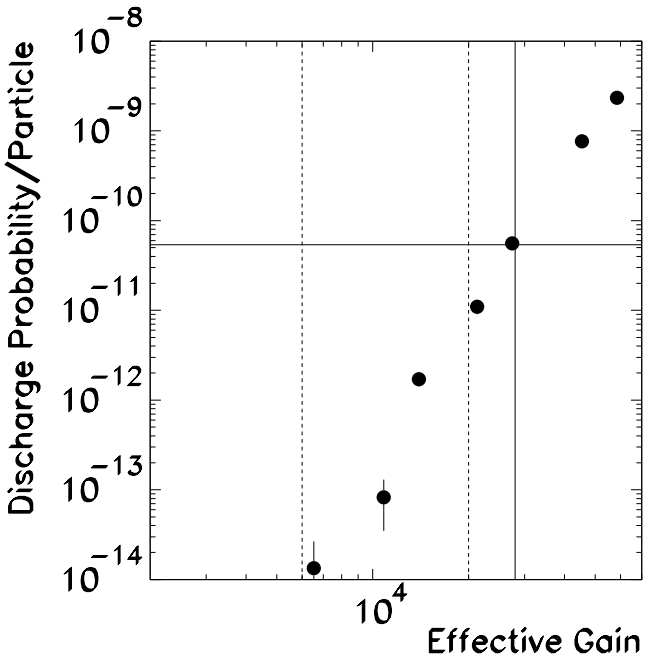

Figure 10 Measured discharge probability per incident charged particle vs. effective gain. The two vertical dotted lines indicate the detector plateau, as is described in section 4.5. The maximum value of discharge probability per incident particle, assuming the average charged particle rate expected in LHCb and 10 years of running, is shown as an horizontal line; the crossing of this line with the measured efficiency gives the maximum effective gain at which the detector can be operated.

A cosmic ray trigger was built, with the photomultipliers screened from the radiation, mainly Compton electrons, with lead bricks. The threshold in the detector was set to 2 fC equivalent delta pulse input.
Figure 11 shows the rate of threshold crossings due to background radiation vs. the effective gain. It is interesting to note that the rate at the effective gain of 6,000 corresponds to about half the average particle rate in LHCb at M1-R1 while the trigger rate at the effective gain of 10,000 corresponds to the maximum particle rate in LHCb at M1-R1. The high voltage current at this gain was about one half of that in M1-R1 of LHCb. We could not put the detector in a higher irradiated region due to technical reasons related to the back-end readout electronics.
Figure 12 shows the time resolution on cosmic rays (Gaussian fit to the time distribution) vs. the effective gain with the radioactive source on (black dots) and off (open dots), indicating that there is no significant deterioration of the time resolution of the chamber due to the presence of background.

5 Ageing studies

With the expected average rate of 184 kHz/cm^2 of charged particles in 10 years, assuming an operating effective gain for of 6000 (see section 4.5), the triple-GEM detector should integrate without damage or performance deterioration about 1C/cm^2.
Local aging tests, either with a high intensity X-ray beam or with the πM1 hadron beam at the Paul Scherrer Institute (PSI), were performed on small size triple-GEM prototypes. In both cases, after an integrated charge equivalent to several years of operation at LHCb, negligible aging effects were observed with all the gas mixtures used [3].
Anyway, due to the large amount of CF_4 (40%) presents in the gas mixture, in order to check the com-

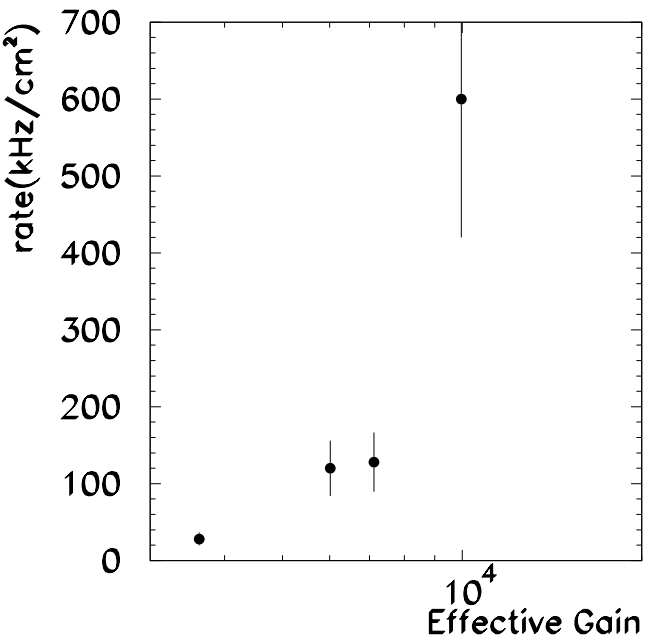

Figure 11 Rate of threshold crossings due to background radiation vs. effective gain in the Enea-Casaccia test.

patibility between the construction materials (for detectors and gas system) and the gas mixture, a global irradiation test of the final chamber is required.

For this reason we performed a test at the Calliope facility of the ENEA-Casaccia, discussed in section 4.7. Three large size prototypes were irradiated on the whole active area at different gamma rates from $\sim$ 1MHz/cm^2 up to $\sim$ 15-20MHz/cm^2. The gas flow rate was 350 cm^3/min, to be compared with the single detector volume of $\sim$ 350 cm^3. The lowest irradiated detector was used as reference chamber and installed upstream in the same gas line of the high irradiated detectors. The whole gas inlet line was made of stainless-steel tubes, while the exhaust gas line was made of polypropylene tubes (not hygroscopic). A probe was directly installed on the gas line, downstream the test chambers, in order to monitor the temperature and humidity of the gas mixture. The water content in the gas mixture was substantially kept under few ppm during the whole test. An additional probe supplied the monitor of the atmospheric pressure.

The total accumulated charges on the three prototypes were $\sim$ 0.08 C/cm^2 for the lowest irradiated detector, $\sim$ 0.8 C/cm^2 and $\sim$ 1.1 C/cm^2 for the highest irradiated ones, corresponding respectively to about 1 (chamber C), 8.5 (chamber B) and 11.5 (chamber A) years of operation at LHCb. At the end of the test the chamber C shows no aging, while current drops of $\sim$89% and $\sim$80% were observed respectively for chamber A and B, Fig. 13.

The result obtained in the global aging test has been attributed to the insufficient gas flow rate (350 cm^3/min, the maximum flow reachable with our mass-flow meters) with respect to the very high gamma rate ($\sim$ 15-20MHz/cm^2 equivalent m.i.p. on the whole detector area, corresponding to a pad current of the order of 400-500 μA) at which chambers were exposed during the irradiation test. On the contrary local tests were performed in completely different experimental conditions: a gas flow rate of 100 cm^3/min for a global detector current of 0.2-0.4 μA (over an irradiated area of the order of 1mm^2).

In this framework we believe that the Casaccia test has been performed in strong gas pollution conditions and then should be considered pessimistic and misleading. In fact, in such test conditions chambers were probably submitted to a strong plasma etching by fluorine, produced in the fragmentation of

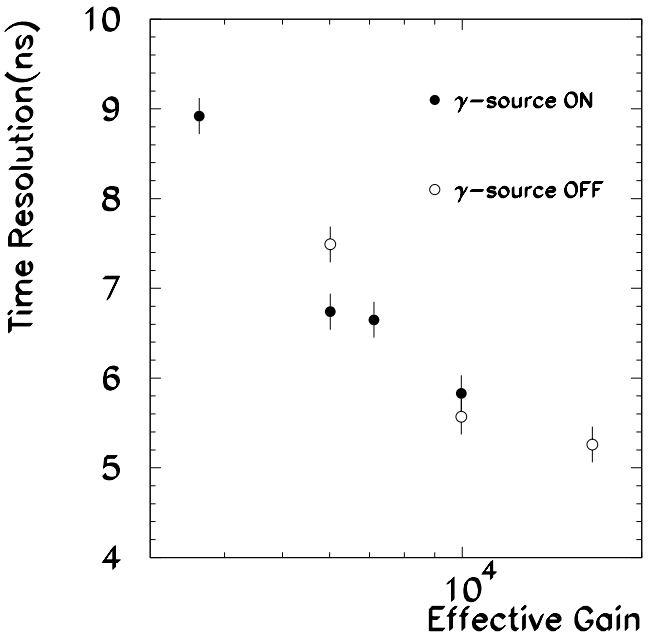

Figure 12 Time resolution on cosmic rays (Gaussian fit to the time distribution) vs. effective gain with (black dots) and without (open dots) the radioactive source on in the Enea-Casaccia test.

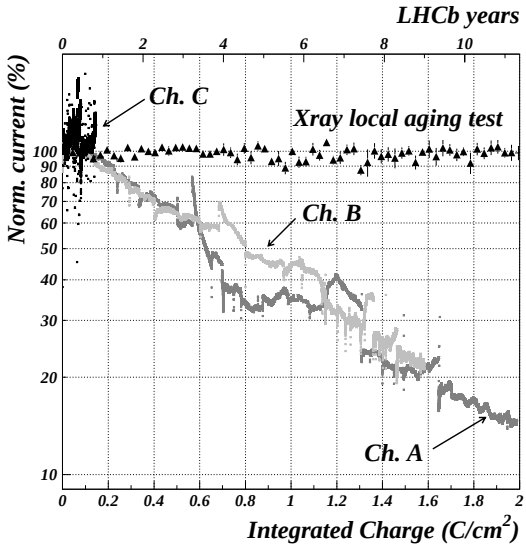

Figure 13 Comparison between local aging, PSI and the global irradiation test at the ENEA-Casaccia.

the CF_4 , and not quickly removed by the gas flow. As a consequence, permanent changes should be found on the GEM foil, in particular on the GEM holes diameter and probably also on the holes shape, especially on the third GEM foil, where the global amplification is larger.
Several checks and measurements successively done on the aged chambers support such hypothesis.

5.1 Beam test results on aged chambers

The two chambers, A and B, were measured before the Casaccia test at the electron beam facility (BTF) of the Frascati Laboratory. After the aging test both chambers have been tested at the PS beam facility at CERN. The results, presented in figure 14, show that aged chambers exhibit practically the same performances, in terms of efficiency in 20 ns, as before their irradiation.

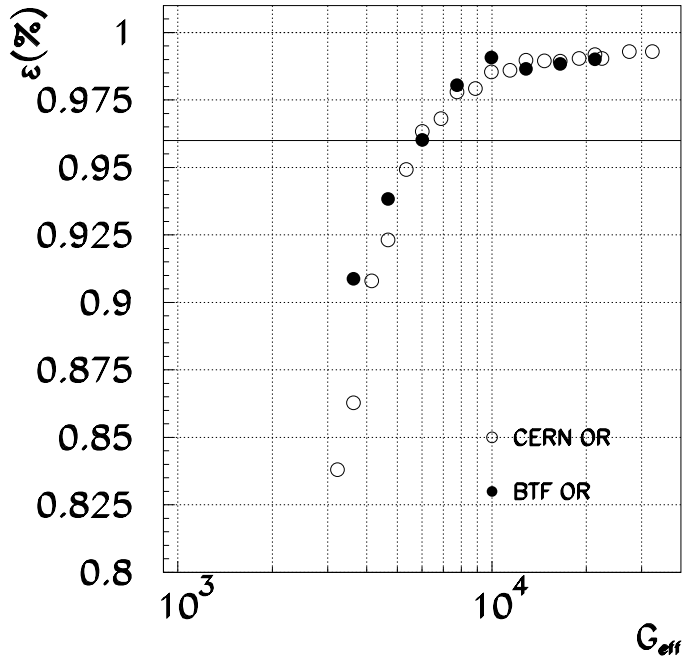

Figure 14 Comparison between the OR-efficiency in 20 ns as measured before (at BTF-LNF) and after (at CERN)the aging test at ENEA-Casaccia.

5.2 SEM analysis and X-rays test results on aged chambers

In order to understand the ageing mechanism occurred during the Casaccia test, a scanning electron microscope (SEM) analysis has been performed on various samples of the aged chambers.

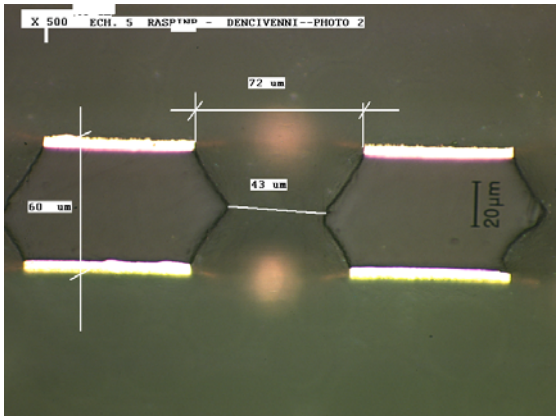

Figure 15 Cross section of the first GEM foil of the aged chamber A. Since, as expected, no etching effects are visibile, the GEM can be considered as a

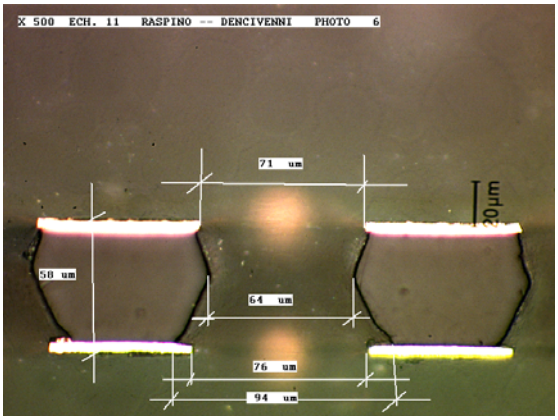

Figure 16 Cross section of the third GEM foil of the aged chamber A. It is clearly visible the etching of the kapton on the bottom part of the hole due to

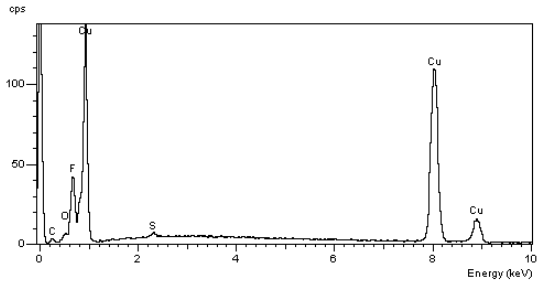

Figure 17 X-ray spectroscopy of the bottom surface of the third GEM foil near the hole edge. The analysis clearly indicates a presence of fluorine.

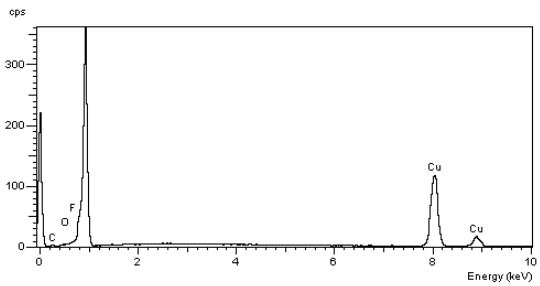

Figure 18 X-ray spectroscopy of the top surface of the third GEM foil near the hole edge. No fluorine has been found in this case.

The results obtained are clearly compatible with a fluorine etching: no polymerization deposits (typical of the so called classical aging) have been observed on the surfaces. As expected the etching effects are larger on the third GEM foil, minor effects are found on the second GEM, while the first GEM does not present any appreciable etching effects. The cathode (drift electrode) and the anode (the pad PCB) are perfectly clean. On both third and second GEMs the observed effect consists in a appreciable widening of the external (copper) holes diameter, from the standard 70 μm up to 80 μm. On the third GEM, where the etching processes were clearly larger, also the kapton inside holes has been etched: the effective holes diameter from the standard 45-50 μm becomes 60-65 μm, Fig. 15 and Fig. 16. Fluorine has been found only on the bottom surface of the third and second GEM, being larger on the third GEM and smaller on the second one. Fluorine is mostly located on the copper near the holes edge, leading to the formation of a thin non conductive layer (a fluorine-copper compound) in proximity of the holes, Fig. 17,Fig. 18.

The enlargement of GEM holes leads to a decrease of the gas gain [10], while the etching of the kapton inside the holes and the non conductive layer on the copper near the hole edge, enhancing charging-up effects, reduce the rate capability of the detector (at very high rate). For chamber A the gas gain reduction measured with X-rays (at relatively low particle rate, $\sim$ 1.6MHz/cm^2) is of the order of 50-55% Fig. 19, while the lost in terms of rate capability, Fig. 20, is at a level of 30% at particle rate of $\sim$ 15MHz/cm^2 (the rate capability is fine up to 3-4 MHz/cm^2, well above the LHCb requirements for M1R1, $\sim$500 kHz/cm^2). These results are compatible with the current drop of 89% observed at the Casaccia test.

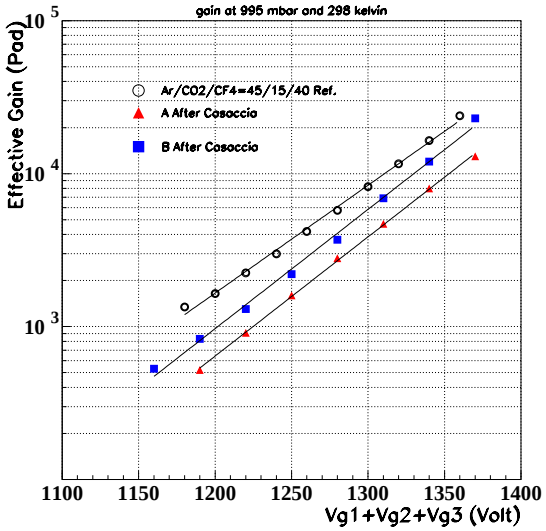

Figure 19 Comparison between the gain measured on a new GEM detector and the gain measured on chamber A and B after the Casaccia aging test.

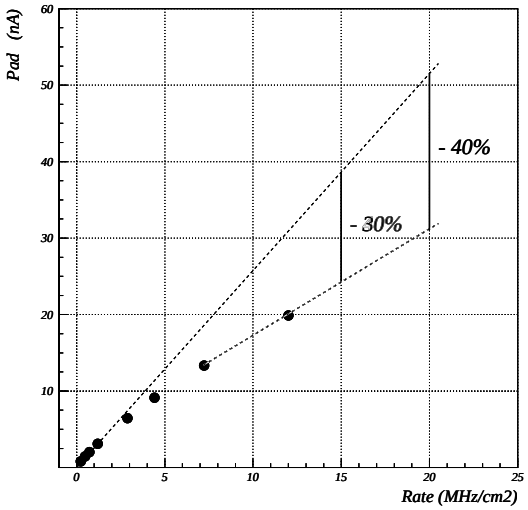

Figure 20 Rate capability of chamber A, measured after the Casaccia test. The measurement has been performed with an X-ray tube.

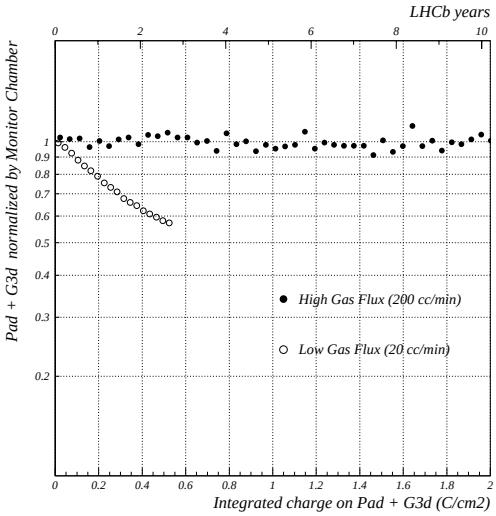

Figure 21 Comparison between the aging measured on a small prototype with low gas flow ($\sim$ 20 cm^3/min) and high gas flow ($\sim$ 200 cm^3/min).

Finally, in order to demonstrate that the etching observed at the Casaccia test was essentially due to an insufficient gas flow rate compared with the high irradiation level, we reproduced such conditions irradiating with a high intensity X-rays beam a 10×10 cm^2 prototype, flushed with a reduced gas flow, Fig. 21. The current drawn by the chamber was about 1 μA on a $1cm^2$ irradiated area, while the gas flow was $\sim$ 20 cm^3/min . In such conditions we observe a gain drop of about 40% in $\sim$3 LHCb equivalent years. The test, repeated with a gas flow of $\sim$ 200 cm^3/min and with a current of 0.5μA on a $1cm^2$

irradiated area, gave a result compatible with no aging in about 10 LHCb equivalent years.

The results of the severe and systematic tests performed on triple-GEM detectors, indicate that the detector is robust and can tolerate the radiation dose foreseen in 10 years of operation in the region M1R1 of the LHCb experiment: detectors, even after a severe irradiation in very bad conditions, exhibit good time and efficiency (in 20 ns) performances, except for a shift of about 20-25 V on the working point, with practically unaffected working ranges.
In addition the results of the Casaccia test, apparently in disagreement with the other aging tests previously performed, have been understood. We have demonstrated that the etching observed during this test is clearly correlated with bad gas flow rate conditions. No aging occur if the gas flow is properly set. In the LHCb running conditions, where the average current collected on pads by one full size chamber will be of the order of 5μA, a safe gas flow rate could be $\sim 100\ cm^3$/min in open mode.

6 Costs

Table 1 Costs of one triple-GEM detector. Prices in CHF.

item	quantity	unit price	total price
Frames	4	54	217
GEM foils	3	387	1162
Pad PCB	1	388	388
Cathode PCB	1	186	186
Honeycomb Panels	2	191	372
Gas connectors	4	8	31
Faraday cage	1	62	62
Glue			15
Total			2430

The total cost for M1R1, constituted by 24 triple-GEM detectors (+ 10% of spares) is estimated to be about 72,850 CHF. The cost of CARDIAC boards (front-end), low voltage boards and HV divider is not included. The cost of electronics is included in table 3 of [2].
Table 1 shows the cost estimate of the various detector components. The cost of the gas system, which consist of mass flow-meters and control unit, pressure-temperature and humidity control system, is estimated to be about 43,400 CHF.

7 Milestones and Project organization

The construction of the detectors is equally shared between INFN-Cagliari and LNF. Both construction sites are fully equipped for the detector construction and testing. LNF has the reponsibility for mechanical design of the detectors, HV divider, LV-boards and the material procurement for detector construction. INFN-Cagliari is responsible for the front-end electronic board design and production and the design and procurement of all the GEM foils.
The construction and testing of the detectors will be completed by the end of 2005. The installation will start early in 2006 and will take a few months, the commissioning of M1R1 is foreseen for September 2006. A detailed schedule is given in figure 22.

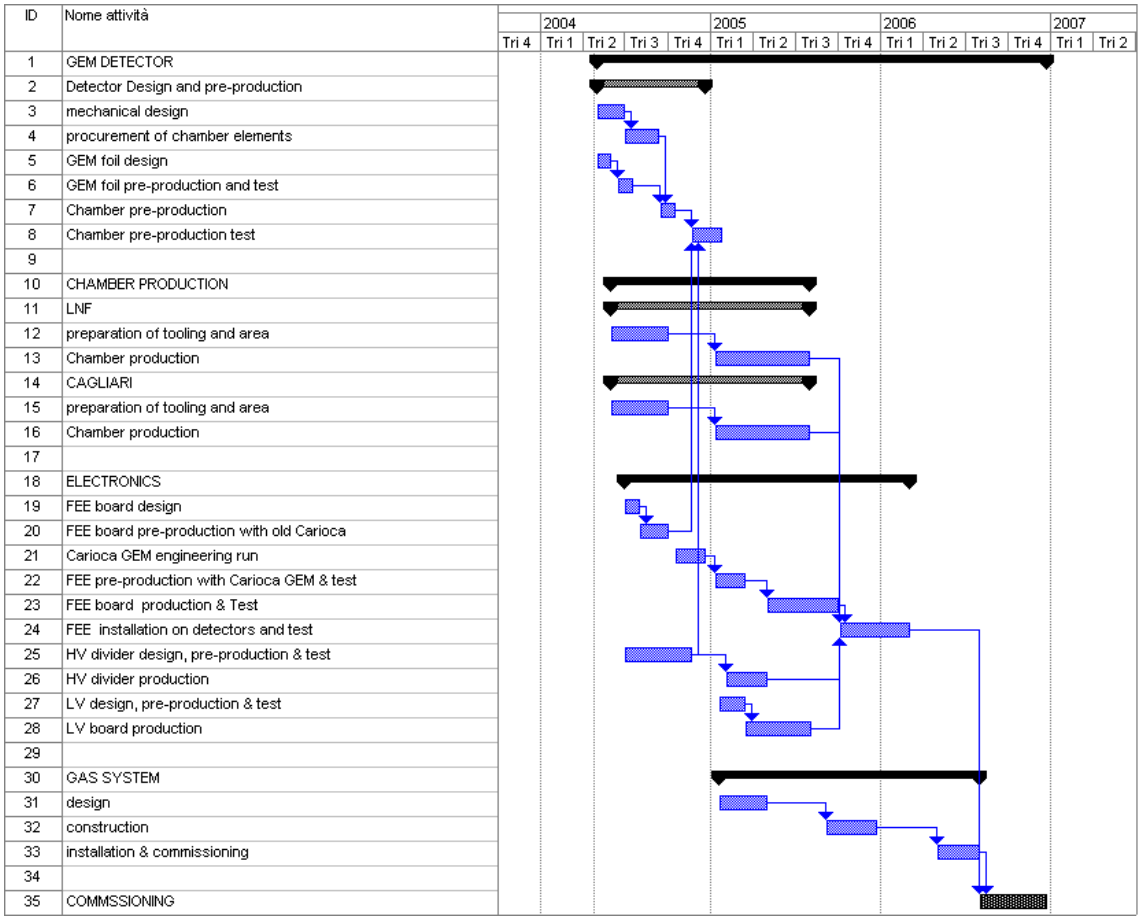

Figure 22 Schedule of the LHCb M1R1 Muon Detector, showing production and installation of detector and electronics.

References

[1] LHCb collaboration, “LHCb Muon System Technical Design Report”, CERN/LHCC 2001-010

[2] LHCb Collaboration, “Addendum to the Muon System Technical Design Report”, CERN/LHCC 2003-002

[3] G. Bencivenni et al., Nucl. Instr. and Meth. A 494 (2002) 156, and references therein. For a complete list see `http://www.lnf.infn.it/esperimenti/lhcb/gem`.

[4] M. Alfonsi, G. Bencivenni, P. de Simone, F. Murtas, M. Poli Lener, B. Sciascia et al., IEEE Trans. Nucl. Sci., accepted for publication, 2004.

[5] B. Bochin, V. Gromov, A. Kashchuck and V. Poliakov, “Signal observation from minimum ionising particles and time resolution estimation in the Triple-GEM detector”, LHCb note 99-099, 1999 [Online]. Available: http://doc.cern.ch//archive/electronic/cern/others/LHB/public/lhcb-99-009.pdf

[6] F. Sauli, “GEM: A new concept for electron amplification in gas detectors,” Nucl. Instrum. Meth. **A386**, 531 (1997).

[7] P. de Simone, M. Alfonsi, G. Bencivenni, M. Poli Lener, W. Bonivento, F. Murtas et al., “Aging measurements on triple-GEM detectors operated with CF4-based mixtures”, presented at the IEEE Nuclear Science Symposium, Rome, Italy, 2004.

[8] W. Bonivento, P. Jarron, D. Moraes, W. Riegler and F. Dos Santos,“Development of the CARIOCA front-end chip for the LHCb muon detector”,Nucl. Instrum. Methods, vol. A491 pp. 233-243, 2002.

[9] M.F. Newcomer, S. Tedja, R. Van Berg, J. Van der Speigel and H.H. Williams,“A fast, low power, amplifier-shaper-discriminator for high rate straw tracking system”,IEEE Trans. Nucl. Sci., vol. 40, pp.630-636, 1993.

[10] S. Bachmann et al., Nucl. Instrum. Meth. **A438** (1999) 376.